Increasing bioelectricity generation in microbial fuel cells by a high-performance cellulose-based membrane electrode assembly

Increasing Bioelectricity Generation In A Single Chamber Microbial Fuel Cell By A Novel Monolithic Structure Membrane Electrode Assembly Based on Low Cost Bacterial Cellulose and Cheap Nano-Zycosil

Mehrdad Mashkour[1,3], Mostafa Rahimnejad[*1], Mahdi Mashkour[2] and Francesca Soavi[3]

[1] Biofuel and Renewable Energy Research Center, Babol Noshirvani University of Technology, Babol, Iran

[2] Laboratory of Sustainable Nanomaterials, Faculty of Wood and Paper Engineering, Gorgan University of Agricultural Sciences and Natural Resources, Gorgan, Iran

[3] Department of Chemistry "Giacomo Ciamician", Alma Mater Studiorum - Università di Bologna, 40126, Bologna, Italy

* Corresponding author Email address: Rahimnejad_mostafa@yahoo.com, Rahimnejad@nit.ac.ir

Tel: +98 (0) 11 32334204; Fax: +98 (0) 11 32334204

Abstract

Herein, a novel monolithic membrane electrode assembly (MEA) air-cathode based on bacterial cellulose (BC), conductive multi-walled carbon nanotubes (CNT) and hydrophobic nano zycosil (NZ) was fabricated for Microbial fuel cell (MFC). BC as a nano-celluloses with oxygen barrier property can prepare anaerobic condition in the sludge. Binder-less coating of CNT on BC avoids expensive binders like poly-tetra fluoro ethylene (PTFE) and Nafion. Also, NZ is here proposed as a very cheap organosilane to make BC's surface hydrophobic and prevents anolyte leakage. It was coated on BC by an easy, fast and direct approach without post treatment. Diluted NZ increased the water contact angle (WCA) from 49˚(BC) to 85˚(BC-NZ) and balanced hydrophobicity and humidity of BC. Electrochemical performance of the BC-CNT-NZ was compared to PTFE- carbon cloth gas diffusion electrode (GDE) in a single chamber MFC (SCMFC). BC-CNT-NZ produced maximum pulse power density of 1790 mW/m^2 that was approximately two times higher than that obtained by GDE (920 mW/m^2). Also, the capacitance of the MEA was 65 mF and much higher than the value for GDE (0.73 mF). Thus, BC-CNT-NZ is suggested as a high performance and cheap substitute for typical hydrophobic PTFE based GDEs in SCMFC.

Keywords: Bacterial cellulose; Nano zycosil; Carbon nanotubes; Monolithic; Membrane electrode assembly; Microbial fuel cell

1. Introduction

Microbial Fuel Cell (MFC) is an emerging technology in the field of sustainable bioelectricity, wastewater treatment and bioelectronics [1, 2]. In MFCs, bacteria as biocatalysts decompose and consume a wide range of organic molecules, simple or complex, present in waste water, while releasing electrons through an external loading, towards the cathode[3, 4]. At the cathode side, electrons are involved in the oxygen reduction reaction (ORR)[5, 6]. In single chamber MFCs (SCMFCs), the air-breathing cathode prevents

anolyte leakage, and also provides ORR sites [7]. Therefore air-cathode plays a vital role in MFC's operation. A large variety of materials and structures have been employed in air-cathode fabrication process [8, 9]. Typical air-breathing cathodes feature a membrane electrode assembly (MEA) design. MEA key components are: i) the conductive substrate where the electrocatalytic reduction of O_2 takes place, and ii) the hydrophobic layer. Carbon paper and carbon cloth are introduced as commercial conductive substrates coated by a mixture of carbon and poly-tetra fluoro ethylene (PTFE) to build gas diffusion electrode (GDE) air-cathodes [10]. High cost PTFE is used to bind the carbon mixture to the substrate. Furthermore, it makes the GDE surface hydrophobic, and hence, prevents leakage [11]. In addition to conductive substrates, non-electrical conductive ones are also used to fabricate MEA air cathodes. A variety of ultrafiltration membranes, proton, cation and anion exchange membranes can be used as MEA substrates. MEA's substrate plays a vital role as a barrier to anolyte leakage and oxygen cross-over and affects proton or cation exchange for MFC operation[12]. Scientists are making effort to find low-cost air cathodes based on cheap materials and obtained by environmentally friendly processes to make MFC technology more practical.

Cellulose has caught the eye of scientists because it is the most widely available biopolymer in the world [13, 14]. Permeability of oxygen through pure nano cellulose materials is very low [15] and it is necessary to mitigate oxygen crossover by air cathode in MFC [16]. Among nano cellulose materials, bacterial cellulose (BC) has received extensive attention due to its three-dimensional porous nano-structural network, high purity, flexibility, high mechanical strength, and excellent tear resistance in aquatic environments[17, 18]. These novel features make BC an excellent green substrate for electrode fabrication in MFC. Conductive polymers coated BC were exploited as cheap bio-anodes in a double chamber MFC (DCMFC), which gave much higher power density response rather than graphite [19, 20]. In other work, flexible conductive BCs were coated with CNT and Gum Arabic binder by drop casting method and low sheet resistance of 1 Ω.cm was reported [21]. CNT has been investigated as an effective nano carbon in MFCs [22, 23]. In recent years, a great interest has being seen in exploiting BC in biofuel cells (BFCs). BC-CNT composites were prepared by vacuum filter method and were utilized as anode and cathode in two chamber

enzymatic fuel cells [24]. Moreover, a BC based proton exchange membrane (PEM) was fabricated by Vilela et al. with poly sulfonic acid treatment and used it in a SCMFC with a hydrophobic micro porous layer (MPL)-carbon cloth air-cathode [25]. The internal resistance of the MFC was high and the open circuit voltage (OCV) of the cell was low. The reason may be the lack of proper BC's connection to the carbon cloth in that work.

Besides abovementioned properties of BC like oxygen cross-over barrier and proton conductivity, a hydrophobic surface of BC is vital for eliminating water leakage to reach an excellent MEA-air cathode based on BC-CNT as a cheap alternative to high cost carbon cloth and PTFE. Several methods were applied to make cellulose hydrophobic such as: acetylation [26] and silanization of cellulose with organosilane groups by complex methods [27-29]. Apart from the materials, nano-zycosil (NZ), a diluted solution of hydroxyalkyl-alkoxy-alkylsilyl, has been introduced as a cheap and commercially accessible organo-silane. Because of its low cost, NZ is suitable for industrial applications [30, 31]. In this study, for the first time BC-CNT-NZ is fabricated as a monolithic MEA in SCMFC. In all previous studies by the scientists, BC was used only as the membrane in presence of PTFE based-GDEs. Here, one side of BC was coated with CNT by using vacuum filter method with no binder. Consequently, only one side of BC's surface became conductive. The conductive surface was in front of the air. The other side of BC was coated with NZ to make a hydrophobic surface and prevent leakage of the sludge in SCMFC. Various characterization methods were applied to investigate the properties of BC-NZ surface as a novel hydrophobic BC membrane. To the best of our knowledge, it is the first time that BC and NZ are used for the fabrication of MFC air cathode. The monolithic structural MEA was expected to show excellent performance in MFC. Resistance, capacitance, catalytic activity and generated power density of the MEA were studied by several electrochemical experiments.

2. Materials and methods

2.1. Fabrication of BC-CNT-NZ MEA

As can be seen in Fig.1 A, a solution containing 10 mg of CNT (Neutrino Noavarane Nano, Iran) and 25 mg of SDS surfactant in 25 mL of Milli-Q water was mixed under 15 min ultrasonic to reach a homogeneous solution of CNT. Thereafter, the solution was poured on BC membrane (Nano-Novin Polymer, Iran) to cover BC by vacuum force of Buchner [32]. Then, the CNT coated BC was placed in ambient temperature for complete drying. Uncoated surface of BC-CNT was covered by NZ-water solution (1:5, v/v) (Zydex Industries, India) with a painting brush and left to dry overnight to yield the hydrophobic BC-CNT-NZ.

2.2. Characterization of BC-CNT-NZ

NZ coating on BC was evaluated by Attenuated Total Reflectance Fourier Transform Infrared spectroscopy (ATR-FTIR) device (Brucker, Germany). Crystallinity was investigated by x-ray diffraction (XRD) (Philips, Germany) and quantified by the Segal equation [33]. Field Emission Scanning Electron Microscopy (FESEM) (TESCAN, Czech Republic) was utilized to investigate the surface morphology. Energy-dispersive x-ray (EDX) (TESCAN, Czech Republic) spectroscopy measurements provided the atomic percentage of the elements. Atomic force microscopy (AFM) (Philips, Germany) was used to calculate the average roughness of the surface (by Nanosurf Easyscan software) [34], Thermo-gravimetric analysis (TGA) (TA Instruments, USA) was carried out to evaluate thermal stability of materials . Contact angle (Sharif Solar, Iran) measurements were performed to investigate the effect of NZ coating on hydrophobicity.

2.3. SCMFC and incubation

A cubic single-chamber MFC (SCMFC) with four windows for different air-cathodes and 250 ml working volume was used in this research (Fig.1 B). Carbon brush (wrapped around two titanium wires with diameter of 2 cm and height of 4 cm) was embedded in the centre of the chamber as anode electrode. BC-CNT-NZ and commercially GDE were used as air-cathodes. The distance of anode from both GDE and new MEA was the same. The system was incubated by anaerobic sludge from hydrolysis stage at biogas plant (Biotech. Sys. Srl, Bologna, Italy). The sludge was diluted 50:50 V/V by phosphate buffer solution

(0.1 M PBS). The surface of each cathode was 2.5 cm in 2.5 cm. A 1 kΩ external resistance was connected to MFC for a week for biofilm formation. Cathode current collector was from stain-less steel mesh. To seal the air-cathode windows of the chamber, the electrode and current collector were sandwiched between two frames of silicon gaskets. The anode inlet was closed by a silicon cap.

2.4. Electrochemical tests

For all the electrochemical tests, a potentiostat/galvanostat (Biologic Science Instruments, France) at LEME was utilized.

The catalytic activity of BC-CNT-NZ and commercial GDE was evaluated in SCMFC in three-electrode mode, i.e. using the cathodes as working electrode, the anode as counter, and inserting an Ag/AgCl reference electrode in the SCMFC chamber.

Linear sweep voltammetries (LSV) were carried out by rotating disk electrode (RDE) at different rpm to investigate the ORR catalytic activity of CNT in circum-neutral electrolyte. In RDE test, the working electrode was a glassy carbon (GC) RDE coated with CNT following the procedure described in ref. [35]. The experiment was done in a standard-three electrode cell filled by 50 ml PBS (0.1 M, pH=7.6) saturated with oxygen before measurements. A Pt counter electrode and an Ag/ACl reference electrode were used.

The LSV curves were analysed to give the Koutecky-Levich (K-L) and Tafel plots (Eq1 and Eq2):

$$\frac{1}{j} = \frac{1}{j_L} + \frac{1}{j_K} = \beta\omega^{\frac{-1}{2}} + \frac{1}{j_K} \quad (1)$$

$$\log j_K = \gamma\eta + \log j_{K_0} \quad (2)$$

Where j_L, j_K and j are limiting, kinetic and measured currents densities respectively. β is the slope of K-L plot and ω represents the angular velocity of electrode. Also, γ is the slope of Tafel plot and η is measured over-potential[36].

Additionally, LSVs were run in two-electrode mode. In this case, the working electrodes the BC-CNT-NZ and GDE cathodes. The anode brush was used as counter and reference electrode.

The polarization curve of the cell ($V_{cathode}$-V_{anode} vs. current density plot) were analyzed to calculate the output power density (P) by Eq.3:

$$P = \frac{(V_C - V_A) \times I}{A_c} \quad (3)$$

Where V_C, V_A, I and A_C represent cathode (V) and anode (V) potentials, cell's current (mA) and cathode surface area (m^2).

During the cell LSV, to evaluate the single electrode polarization behavior, the electrode potential was simultaneously monitored vs Ag/AgCl in parallel. LSV scan rate was 0.2 $mV.s^{-1}$.

Cyclic voltammetry was performed to evaluate the capacitive behavior of the cathodes. Scan rate was 10 mV s^{1-} and the potential window was -0.3V to 0.3V vs Ag/AgCl. Capacitance was calculated by the slope of the plot of the current integrated over time vs. electrode potential. EIS of cathodes was performed in the frequency range 100 KHz to 20 mHz at OCV. Both CV and EIS were carried out by a three electrode-setup in SCMFC filled with the sludge.

For Galvanostatic (GLV) test, different pulse current (I_{pulse}) were imposed to discharge MFC in various pulse times (t_{pulse}): 0.1s, 0.5s, 1s and 2s. After each discharge, the SCMFC was left to rest in OCV until a stable voltage was reached. In this method, cell voltage, anode and cathode potentials were recorded versus reference electrode (Ag/AgCl) and plotted vs. time. The pulse power (P_{Pulse}) was calculated by the cell GLV discharge according to Eq.4 [37-39]:

$$P_{pulse}=(I_{pulse}*\int_0^t Vdt)/t_{pulse} \quad (4)$$

3. Results and discussion

3.1. Surface Chemistry of BC-NZ

ATR-FTIR spectra of BC and BC-NZ films are reported in Fig.2 A. To reach a complete and qualitative comparison by FTIR spectra, the absorbance range was splitted to 4000-2500 cm^{-1} and 1500-500 cm^{-1}. A successful treatment of BC by NZ was found by the bands that can be detected at 775 cm^{-1} and 1270 cm^{-1} which can be attributed to bending vibrations of Si-CH_3 [28]. Additionally, stretching vibration of Si-CH_3 was visible by a small peak at 2966 cm^{-1} [27, 40]. The latest peak located near 3000 cm^{-1} provided evidence of the hydrophobic feature of BC. Also, the sharp signal between 1025 cm^{-1} and 1035 cm^{-1} can be attributed to Si-O bond [41]. In this region, it can be observed even a signal related to C-O deformation of cellulose (overlapping with Si-O of alkoxy group). Therefore, the normalized intensity of the peak at 898 cm^{-1} for both BC and BC-NZ was compared and resulted 1.26 and 1.42 for BC and BC-NZ, respectively. As a consequence, increased intensity of the peak for BC-NZ was related to Si-O bond.

The fingerprint region between 1500-700 cm^{-1} is of great importance in identifying structural changes of BC. Crystalline structure of BC was surveyed by two main indexes: total crystalline index (TCI) and lateral order index (LOI) [42, 43]. TCI and LOI were calculated by the ratio of A_{1372}/A_{2920} and A_{1430}/A_{898} respectively for both BC and BC-NZ. Bands at 1430 cm^{-1} and 898 cm^{-1} are representatives for crystalline and amorphous structure of BC[44]. Decrease in both LOI and TCI (Table 1) showed that a slight reaction between BC and nano zycosil has degraded a little the ordered structure of BC and its crystallites. Additionally, hydrogen bond index (HBI) which is defined as A_{3340}/A_{1330} was evaluated for both samples and then no noticeable change in HBI was observed (Table 1). Hence, the change in –OH group of BC was not significant. This behavior was mentioned earlier by Zanini et al. and Sai et al. for silanized cellulose [27, 45].

Besides ATR-FTIR spectra, EDX analysis (Fig.2 B) was also performed to study atomic distribution on the surface of BC-NZ. The results showed 2.43% of surface atoms were Si. Additionally, by EDX mapping, it was found that a homogenous coating of Si atoms occurred on BC's nano fibers. As it was mentioned, the main reason of NZ coating was making a hydrophobic surface of BC.

3.2. Crystallinity and thermal stability of BC-NZ

BC crystallinity was proven by the presence of the diffraction peaks at 2θ 22.8°, 17.8°and 15°corresponding to the planes 200, 110 and 110 (Fig.2 C) respectively [19, 20]. To investigate the effect of NZ on BC nanofibers, the crystallinity of both pure and treated BC was calculated by Segal equation. Crystallinity of 92% and 87% for BC and BC-NZ indicates a negligible effect of silane groups on BC crystal structure. This result confirmed the small decrease in TCI and LOI detected by ATR-FTIR spectra and commented in the previous section. Accordingly, both FTIR and XRD analyses verified each other.

TGA and its differentiation (DTG) curves of BC and BC-NZ are displayed in Fig.2 D. Below 100℃, the TGA curves exhibited a weight loss associated with the evaporation of sample's moisture (3.5%). The main BC' degradation took place at the range of 320 to 340℃. DTG curves showed that after treatment by NZ, the maximum rate of BC's decomposition occurred at higher temperature (it shifted from 321℃ for BC to 338℃ for BC-NZ). Furthermore, the rate was smaller in the case of BC-NZ. Hence, thermal analysis suggests that silane groups of NZ improved the thermal stability of BC's nano fibers. This result is in agreement with previous BC silanization [27].

3.3. Surface morphology, hydrophobicity, roughness and barrier properties of BC-NZ

FE-SEM images of BC before and after modification are visible in Fig.3. By comparing Fig.3 (A and B) corresponding to bare BC and BC-NZ, it is obvious that BC' surface was covered considerably by NZ and also the pores between fibres became smaller. Therefore, the morphology change shown in FESEM suggests that treatment with NZ should improve the barrier property of BC. WCA as a criteria for hydrophobicity was measured. An appreciable change was seen between WCA of bare (49°) and NZ treated

BC (85°) (insets of Fig.3 (A and B)). Higher WCA resulted in higher hydrophobicity and also improved water leakage barrier of BC-NZ membrane. It is noticeable that 98% w/w of bare BC in wet state is formed from water. Hence, BC without surface treatment has considerable leakage followed by its high affinity to water and cannot be applied as a separator or membrane in air-cathode fabrication. FE-SEM images and WCA confirmed successful surface treatment of BC by NZ. Additionally, AFM images (Fig. 3 (C and D)) showed that surface roughness was decreased from 45.66 nm for BC to 32.51 nm for BC-NZ. Also, the values of valley depth and peak height showed decrease after treatment of BC with NZ. It means that BC's pores with micron scale have become filled with NZ[46, 47]. It was also clear in FESEM images. Hence, all AFM, FFSEM and WCA results implied on hydrophobic features of treated BC.

It is necessary to know BC's desired hydrophobization degree for MEA. A balanced WCA presents better performance. This theory was brought up previously for GDL of air-cathode by Ci et al [11]. To the best of our knowledge, here it is the first time that the theory is considered for MEAs. As can be seen in Fig.4 A, ORR needs sufficient protons, electrons and oxygen. For introduced BC-CNT-NZ, protons cross BC-NZ to meet electrons and oxygen at the interface of BC and CNT. High WCA (130°) decreases total protons reaching the BC-CNT interface and therefore makes a limiting factor to ORR. On the other hands, low WCA (49°) results in leakage and therefore lower concentration of oxygen in ORR sites (because of lower soluble oxygen in water phase rather than air). Thus, a balanced WCA (85°) not only provides sufficiently proton transfer in reaction sites by BC but also prevents leakage by NZ coating. Furthermore, performance of BC-NZ as a barrier to air oxygen penetration was evaluated by measuring dissolved oxygen (DO) (by DELTA OHM, Italy) versus time and was compared with the measured amount of PTFE based GDE and Mylar (as control) (Fig. 4 B). The experiment was carried out in three similar cells with BC-NZ, PTFE and Mylar respectively, all filled by PBS (initially purged with nitrogen for 30 minutes to remove DO). After 9 h, the cell with BC-NZ showed a plateau in low DO while the GDE showed a growing trend. Hence, excellent anaerobic condition was provided by new MEA. Indeed, NZ provided both hydrophobicity and great barrier property against oxygen diffusion. It is a positive point for use of NZ rather than PTFE. The

other parameter in SCMFC is anolyte evaporation rate from air-cathode surface. For this purpose, the three cells were weighted in a period of 90 h to find weight-loss associated with evaporation of PBS (Fig. 4 C). The behavior of both BC-NZ and PTFE based GDE was almost same. A little higher rate of BC-NZ may be explained by the mentioned balance between hydrophobicity and humidity in BC-NZ.

3.4. Electrochemical properties of BC-CNT-NZ compared to commercial GDE

3.4.1. Impedance spectroscopy study

EIS spectra of BC-CNT-NZ and commercial GDE are demonstrated in Fig.5. The Nyquist diagram of BC-CNT-NZ span in an impedance range that is much smaller than that of the GDE and is not visible without magnification. At 20 mHz, real and imaginary parts of impedance were 114.283 Ω and 122.28 Ω respectively for BC-CNT-NZ while GDE showed much higher resistances, 2.8 kΩ and 10.8 kΩ respectively. At the high frequency range, BC-CNT-NZ Nyquist plot features a semicircle that can be related to the electronic connection between the CNT and the stainless steel current collector. In the middle frequency range, a line with a slope approaching 45º is representative of ion diffusion in to the BC-CNT-NZ porous architecture, and can be modelled with a Warburg element. Additionally, in low frequency region, BC-CNT-NZ's capacitive behavior appears much more prominent rather than its Warburg part. [48, 49]. The BC-CNT-NZ's capacitive response at the lowest frequency of 20 mHz is 65 mF. This value was evaluated by the Eq.5:

$$C=1/Z_i 2\pi f \quad (5)$$

Where Z_i is the imaginary component of the impedance at the frequency f. On the other hand, for GDE, the capacitive response evaluated at 20 mHz by eq. 5 is 733 μF. Therefore, EIS showed that both resistance and capacitance of BC-CNT-NZ electrodes are better than GDE.

3.4.2. LSV and CV tests

The LSV reported in Fig.6 A indicates that for BC-CNT-NZ the ORR onset potential is at least 100 mV higher than GDE. This is beneficial to achieve a high SCMFC voltage operation. Additionally, the cellulosic cathode produced much more current over the voltage range investigated. At -0.3 V vs Ag/AgCl, a current of 0.75 mA was achieved. Furthermore, the slope of linear part of the LSV was higher for BC-CNT-NZ, in agreement with its lower impedance evaluated by EIS. These findings indicate that BC-CNT-NZ can be a suitable air-cathode that features higher catalytic activity than GDL. The purpose of CV analysis was the evaluation of the capacitive performance of the electrodes (Fig.6 B).The voltammetric currents of BC-CNT-NZ's are dramatically higher than those of the GDE, therefore indicating a higher capacitance of the former electrode with respect to the latter. Indeed, the capacitance resulted of 84.44 mF and 2.47 mF for BC-CNT-NZ and GDL, respectively. Therefore, CNT is effective in providing to BC both the suitable electrical conductivity for current collection and also acceptable capacitive behaviour. Thus, LSV and CV gave indications about the catalytic activity and capacitive properties of BC-CNT-NZ.

3.4.3. Power density and polarization tests

Fig.6 C report the LSV polarization (V-I) and power (P-I) curves of SCMFC assembled with BC-CNT-NZ and GDL cathodes. The SCMFC could produce a maximum power density of about 80 mW/m^2 in presence of BC-CNT-NZ that was three times higher than the power delivered by the cell with the GDE cathode (25 mW/m^2). The OCVs were almost the same for the two cells. However, the initial voltage drop at the lowest currents of the SCMFC with the GDE was much higher than BC-CNT-NZ. Also the slope of the linear part of the polarization curve at the middle-high currents was lower. These two features are in agreement with the higher resistance and lower capacitance of the GDE vs. the BC-CNT-NZ cathode. To make this improvement more clear, single electrode potentials were monitored during the polarization tests, and the results are reported in Fig.6 D. The anode behaviour was similar for the two cells, but the GDL cathode showed higher voltage drop at the lowest currents and higher slope at the middle-high currents with respect to the BC-CNT-NZ. This indicates the overall SCMFC response is mainly affected by the cathode performance and it is improved by the substitution of GDL with BC-CNT-NZ. In this work, it was a

noteworthy point that making a homogenous junction between BC and CNT resulted in a minimum ohmic drop in MFC. Previously maximum power density of 2.42 $mW.m^{-2}$ was reported by using treated BC as a membrane for conventional carbon cloth based GDE [25]. The low power may be attributed to poor connection of BC to GDE. Hence, our results demonstrate that by our approach we succeeded in producing an effective BC based, monolithic MEA air cathode. The CNT layer exposed to air (Fig. S1) provided a good access to oxygen and showed interesting ORR electrocatalytic response. In parallel, the NZ coating exposed to the anolyte played the role of membrane and separator preventing leakage by a well-balanced wettability and hydrophobicity. Moreover, durability of binder-less CNT coating was already demonstrated in previous reports [24, 32]. In this work, after more than two months, the coating was not defected and did not release.

3.4.4. RDE experiments

To get insight into ORR electrocatalytic activity of BC-CNT-NZ, CNT modified glassy carbon (GC) and bare GC electrodes were studied by RDE in oxygen saturated buffer solution. Fig. 7 A shows the RDE LSVs at 5 mV/s and 0, 400, 900, 1600 and 2500 rpm. The CNT-GC RDE current density is a combination of capacitive and faradic components. The LSV curves were analysed to give the K-L plots (reported in Fig. 7 B) in a potential range where the response is affected both by kinetic and mass transfer limitations. In order to eliminate the contribution of the capacitive currents, at each potential the LSV current density was subtracted by the value measured in Ar-saturated solution. The slope of the K-L plots (β) (Eq. 2) depends on the number of electron transferred in the ORR process [35]. Higher slope corresponds to a lower number of electrons. The K-L slope for CNT-GC is 1.84 and lower than that obtained with bare GC (Fig. S2, 3.56). This indicates that CNT could increase the number of electron transferred in ORR with respect to GC. Furthermore, the slope of Tafel plot (inset of Fig. 7 A) for CNT-GC was 6.15 and lower than that of GC (10.91).All the data for bare GC electrode is visible in Supplementary file Fig. S2 A & B.

3.4.5. GLV discharge tests

Fig.8 reports the power delivered by the SCMFC evaluated by GLV discharges with pulse time of 0.1, 05, 1 and 2 s. This kind of power curve can show brightly the potential application of MFC as a power supply for an electronic consumer. The highest pulse power values of 800, 1030, 1210 and 1790 mW/m^2 can be achieved at currents of 1.6, 2.2, 2.8 and 4 mA for the MFC with BC-CNT-NZ cathode. This cell delivers around two fold higher power than that of the cell with the GDE. Also, it was shown that by decreasing pulse time, the generated power was further boosted.

3.5. BC-CNT-NZ as a monolithic MEA versus cellulosic membrane and air-cathodes: performance and properties in MFC

Table 2 provides details of using cellulose in fabricating membrane and air-cathodes in MFCs. Biffinger et al. used cellulose nitrate at a mini DCMFC with graphite felt as anode and cathode. In the work cellulosic membrane showed lower power density (40 $mW.m^{-2}$) than that by Nafion [50]. In other work, BC was utilized in a huge DCMFC as proton exchange membrane with carbon plate electrodes. The system could increase power density more than two folds rather than that by commercial cation exchange membrane.it showed high potential of bacterial cellulose as a cheap alternative to expensive Nafion [51]. Ci et al. treated cellulose by esterification and then used it in behalf of PTFE hydrophobic layer on carbon cloth air cathode. They could improve MFC performance by the substitution and also decrease the cost of air-cathode by elimination of PTFE. Although, they used platinum as catalyst which is not economical for MFC technology[11]. Also, cellulose was not applied as membrane in the work. In other research, Wang et al. put a mixed cellulose ester membrane between platinum catalyst layer on GDE and anolyte. The separator layer's performance was similar to Nafion's[52]. In 2017, Marzorati et al. used the cellulosic shell of Maize stalks as separator in a cylindrical SCMFC on commercial GDE-carbon black and reached power density of 44 $mW.m^{-2}$ [53]. In the work diameter of Maize stalk was limiting factor for MFC size. More recently, Vilela et al. in 2019 synthesized Poly (4-styrene sulfonic acid) treated BC as a separator in a SCMFC which produced 2.42 $mW.m^{-2}$ with platinum coated GDE[54]. All aforementioned GDEs were fabricated by high cost PTFE as hydrophobic agent and Nafion or PTFE as binder for catalyst coating. Also, the cellulosic

membranes as separators were apart from GDEs and there was not homogeneous contact between membranes and GDEs unlike the monolithic MEA in this work. It should be noted that for a fair comparison of the mentioned cellulose based MFCs' performance, it is necessary to consider power measurement method. Resistance loading, LSV and galvanostatic discharge are different methods for measuring output power of MFC. Reported output power may differ because of different values of parameters such as: scan rate, resistance values, discharge current and pulse time. For example Ci et al. used resistance loading and did not mention pulse time of each loading, while Vilela et al. used discharge test with pulse currents of 5 μA and pulse time of 3 minutes. It may be the reason of considerable differences between the power density values in Table 2. In this work, in order to report power density, LSV test and GLV discharge gave rise maximum power densities of 80 $mW.m^{-2}$ and 1790 $mW.m^{-2}$ respectively which is higher than that of previous reports. Other improvement in this work by fabricating a homogenous and monolithic BC based MEA, was eliminating both carbon cloth and PTFE which means decreasing the cost of MFC. Cheap NZ was used for the first time for cellulose hydrophobization by a very easy method of coating, CNT was coated as both conductive carbon and catalyst instead of high cost platinum by a binder-less method. This monolithic MEA could prevent anolyte leakage. In addition to explained DO experiment, by a simple lectrochemical test it was proved that the MEA is an excellent oxygen barrier. With reversing the face of electrode (CNT face to anolyte side and NZ face to air) the open circuit voltage of cathode showed downward trend and reached -0.37 V after 20 days of MFC operation. It implied on non-availability of oxygen in sludge. It was expected from BC as a nano-cellulose oxygen barrier. Thus, BC-NZ demonstrated an excellent role as oxygen barrier to prepare anaerobic condition in anolyte of MFC.

4. Conclusions

To the best of our knowledge, a monolithic MEA based on hydrophobic BC was fabricated for the first time and it was used as MFC's air-cathode. Very simple coating method was exploited for hydrophobization of BC by the cheap NZ for the first time. NZ coating made a balance between hydrophobicity and wettability of BC. Afterward, the electrode performance as an air-cathode was compared with a commercial GDE with

PTFE based hydrophobic layer in a SCMFC. EIS showed much lower impedance of BC-CNT-NZ rather than GDE. Also, LSV and CV in agreement with EIS, showed higher catalytic activity and much higher capacitive behaviour of cellulosic cathode. In LSV test, BC-CNT-NZ boosted power density by 320% in comparison with that of commercial PTFE-carbon cloth GDE. It is the best performance of a cellulosic MEA ever achieved at MFC. Thus, using cheap NZ for hydrophobization of BC showed it is an excellent alternative to PTFE.

Acknowledgement

The authors would like to thank Carlo Santoro for his great help in this research. Also, MM and FS would like to thank Catia Arbizzani and Federico Poli at Laboratory of Electrochemistry of Materials for Energetics (LEME) (Bologna-Italy). This work was supported by Iran National Science Foundation (INSF), grant number: INSF-95819857, Biofuel & Renewable Energy Research Center, Babol Noshirvani University of Technology (grant number: BNUT/5150010/1394) and University of Bologna. Also, the research has been carried out under the Italy-South Africa joint Research Programme 2018-2020, Italian Ministers of Foreign Affairs and of the Environment. Moreover, the authors thank Danesh Gostar Hamgam ba Sanat spin-off (Babol, Iran) for facilities and supports.

References

[1] Rahimnejad M, Ghoreyshi AA, Najafpour G, Jafary T. Power generation from organic substrate in batch and continuous flow microbial fuel cell operations. Appl. Energy. 2011;88:3999-4004.
[2] Santoro C, Arbizzani C, Erable B, Ieropoulos I. Microbial fuel cells: from fundamentals to applications. A review. J. Power Sources. 2017;356:225-44.
[3] Xiong J, Hu M, Li X, Li H, Li X, Liu X, et al. Porous graphite: A facile synthesis from ferrous gluconate and excellent performance as anode electrocatalyst of microbial fuel cell. Biosens. Bioelectron. 2018;109:116-22.
[4] Trapero JR, Horcajada L, Linares JJ, Lobato J. Is microbial fuel cell technology ready? An economic answer towards industrial commercialization. Appl. Energy. 2017;185:698-707.
[5] Mashkour M, Rahimnejad M, Pourali S, Ezoji H, ElMekawy A, Pant D. Catalytic performance of nano-hybrid graphene and titanium dioxide modified cathodes fabricated with facile and green technique in microbial fuel cell. PRO NAT SCI-MATER. 2017;27:647-51.
[6] Zhang S, Su W, Wang X, Li K, Li Y. Bimetallic metal-organic frameworks derived cobalt nanoparticles embedded in nitrogen-doped carbon nanotube nanopolyhedra as advanced electrocatalyst for high-performance of activated carbon air-cathode microbial fuel cell. Biosens. Bioelectron. 2019;127:181-7.
[7] Kodali M, Herrera S, Kabir S, Serov A, Santoro C, Ieropoulos I, et al. Enhancement of microbial fuel cell performance by introducing a nano-composite cathode catalyst. Electrochim. Acta. 2018;265:56-64.
[8] Zhong K, Li M, Yang Y, Zhang H, Zhang B, Tang J, et al. Nitrogen-doped biochar derived from watermelon rind as oxygen reduction catalyst in air cathode microbial fuel cells. Appl. Energy. 2019;242:516-25.

[9] Wang Z, Mahadevan GD, Wu Y, Zhao F. Progress of air-breathing cathode in microbial fuel cells. J. Power Sources. 2017;356:245-55.
[10] Santoro C, Agrios A, Pasaogullari U, Li B. Effects of gas diffusion layer (GDL) and micro porous layer (MPL) on cathode performance in microbial fuel cells (MFCs). Int. J. Hydrogen Energy. 2011;36:13096-104.
[11] Ci J, Cao C, Kuga S, Shen J, Wu M, Huang Y. Improved performance of microbial fuel cell using esterified corncob cellulose nanofibers to fabricate air-cathode gas diffusion layer. ACS Sustainable Chem. Eng. 2017;5:9614-8.
[12] Jwa E, Yun Y-M, Kim H, Jeong N, Park S-C, Nam J-Y. Domestic wastewater treatment in a tubular microbial electrolysis cell with a membrane electrode assembly. Int. J. Hydrogen Energy. 2019;44:652-60.
[13] Chouler J, Cruz-Izquierdo Á, Rengaraj S, Scott JL, Di Lorenzo M. A screen-printed paper microbial fuel cell biosensor for detection of toxic compounds in water. Biosens. Bioelectron. 2018;102:49-56.
[14] Mashkour M, Kimura T, Mashkour M, Kimura F, Tajvidi M. Printing Birefringent Figures by Surface Tension-Directed Self-Assembly of a Cellulose Nanocrystal/Polymer Ink Components. ACS Appl. Mater. Interfaces. 2018;11:1538-45.
[15] Aulin C, Gällstedt M, Lindström T. Oxygen and oil barrier properties of microfibrillated cellulose films and coatings. Cellulose. 2010;17:559-74.
[16] Oliot M, Etcheverry L, Mosdale A, Basséguy R, Delia M-L, Bergel A. Separator electrode assembly (SEA) with 3-dimensional bioanode and removable air-cathode boosts microbial fuel cell performance. J. Power Sources. 2017;356:389-99.
[17] Mashkour M, Moradabadi Z, Khazaeian A. Physical and tensile properties of epoxy laminated magnetic bacterial cellulose nanocomposite films. J. Appl. Polym. Sci. 2017;134:45118.
[18] Vilela C, Silvestre AJ, Figueiredo FM, Freire CS. Nanocellulose-based materials as components of polymer electrolyte fuel cells. J. Mater. Chem. A. 2019;7:20045-74.
[19] Mashkour M, Rahimnejad M, Mashkour M. Bacterial cellulose-polyaniline nano-biocomposite: a porous media hydrogel bioanode enhancing the performance of microbial fuel cell. J. Power Sources. 2016;325:322-8.
[20] Mashkour M, Rahimnejad M, Mashkour M, Bakeri G, Luque R, Oh SE. Application of wet nanostructured bacterial cellulose as a novel hydrogel bioanode for microbial fuel cells. ChemElectroChem. 2017;4:648-54.
[21] Mashkour M, Sharifinia M, Yousefi H, Afra E. MWCNT-coated cellulose nanopapers: Droplet-coating, process factors, and electrical conductivity performance. Carbohydr. Polym. 2018;202:504-12.
[22] Mahrokh L, Ghourchian H, Nealson KH, Mahrokh M. An efficient microbial fuel cell using a CNT–RTIL based nanocomposite. Carbohydr. Polym. 2017;5:7979-91.
[23] Ghasemi M, Ismail M, Kamarudin SK, Saeedfar K, Daud WRW, Hassan SH, et al. Carbon nanotube as an alternative cathode support and catalyst for microbial fuel cells. Appl. Energy. 2013;102:1050-6.
[24] Li X, Lv P, Yao Y, Feng Q, Mensah A, Li D, et al. A novel single-enzymatic biofuel cell based on highly flexible conductive bacterial cellulose electrode utilizing pollutants as fuel. Chem. Eng. J. 2020;379:122316.
[25] Vilela C, Cordeiro DM, Boas JV, Barbosa P, Nolasco M, Vaz PD, et al. Poly (4-styrene sulfonic acid)/bacterial cellulose membranes: Electrochemical performance in a single-chamber microbial fuel cell. Bioresour. Technol. Rep. 2019:100376.
[26] Mashkour M, Afra E, Resalati H, Mashkour M. Moderate surface acetylation of nanofibrillated cellulose for the improvement of paper strength and barrier properties. RSC Adv. 2015;5:60179-87.
[27] Sai H, Fu R, Xing L, Xiang J, Li Z, Li F, et al. Surface modification of bacterial cellulose aerogels' web-like skeleton for oil/water separation. ACS Appl. Mater. Interfaces. 2015;7:7373-81.
[28] Zanini M, Lavoratti A, Lazzari LK, Galiotto D, Pagnocelli M, Baldasso C, et al. Producing aerogels from silanized cellulose nanofiber suspension. Cellulose. 2017;24:769-79.
[29] Chantereau G, Brown N, Dourges M-A, Freire CS, Silvestre AJ, Sebe G, et al. Silylation of bacterial cellulose to design membranes with intrinsic anti-bacterial properties. Carbohydr. Polym. 2019;220:71-8.
[30] Taghiyari HR. Nano-zycosil in MDF: gas and liquid permeability. Eur. J. Wood Wood Prod. 2013;71:353-60.
[31] Gupta B, Shah D, Mishra B, Joshi P, Gandhi VG, Fougat R. Effect of top soil wettability on water evaporation and plant growth. J. Colloid Interface Sci. 2015;449:506-13.
[32] Lv P, Feng Q, Wang Q, Li D, Zhou J, Wei Q. Preparation of bacterial cellulose/carbon nanotube nanocomposite for biological fuel cell. Fibers Polym. 2016;17:1858-65.
[33] Nam S, French AD, Condon BD, Concha M. Segal crystallinity index revisited by the simulation of X-ray diffraction patterns of cotton cellulose Iβ and cellulose II. Carbohydr. Polym. 2016;135:1-9.
[34] DeGarmo EP, Black JT, Kohser RA, Klamecki BE. Materials and process in manufacturing: Prentice Hall Upper Saddle River; 1997.
[35] Malaie K, Jeyabharathi C, Wulff H, Ganjali MR, Soavi F, Scholz F. Simple preparation of carbon–bimetal oxide nanospinels for high-performance bifunctional oxygen electrocatalysts. New J. Chem. 2018;42:20156-62.
[36] Bard AJ, Faulkner LR, Leddy J, Zoski CG. Electrochemical methods: fundamentals and applications: wiley New York; 1980.
[37] Santoro C, Soavi F, Serov A, Arbizzani C, Atanassov P. Self-powered supercapacitive microbial fuel cell: the ultimate way of boosting and harvesting power. Biosens. Bioelectron. 2016;78:229-35.

[38] Houghton J, Santoro C, Soavi F, Serov A, Ieropoulos I, Arbizzani C, et al. Supercapacitive microbial fuel cell: Characterization and analysis for improved charge storage/delivery performance. Bioresour. Technol. 2016;218:552-60.
[39] Santoro C, Abad FB, Serov A, Kodali M, Howe KJ, Soavi F, et al. Supercapacitive microbial desalination cells: new class of power generating devices for reduction of salinity content. Appl. Energy. 2017;208:25-36.
[40] Phuong HT, Hong NKD, Ngo DT. Study on surface modification of nanosilica aerogel for oil adsorption on surface oil polluted water. Vietnam J. Chem. 2016;54:426-30.
[41] Siuda J, Perdoch W, Mazela B, Zborowska M. Catalyzed Reaction of Cellulose and Lignin with Methyltrimethoxysilane—FT-IR, 13C NMR and 29Si NMR Studies. Materials. 2019;12:2006.
[42] Tsalagkas D, Lagaňa R, Poljanšek I, Oven P, Csoka L. Fabrication of bacterial cellulose thin films self-assembled from sonochemically prepared nanofibrils and its characterization. Ultrason. Sonochem. 2016;28:136-43.
[43] Mashkour M, Tajvidi M, Kimura F, Yousefi H, Kimura T. Strong highly anisotropic magnetocellulose nanocomposite films made by chemical peeling and in situ welding at the interface using an ionic liquid. ACS Appl. Mater. Interfaces. 2014;6:8165-72.
[44] Tabarsa T, Sheykhnazari S, Ashori A, Mashkour M, Khazaeian A. Preparation and characterization of reinforced papers using nano bacterial cellulose. Int. J. Biol. Macromol. 2017;101:334-40.
[45] Poletto M, Zattera AJ, Santana RM. Structural differences between wood species: evidence from chemical composition, FTIR spectroscopy, and thermogravimetric analysis. J. Appl. Polym. Sci. 2012;126:E337-E44.
[46] Kannangara D, Shen W. Roughness effects of cellulose and paper substrates on water drop impact and recoil. Colloids Surf., A. 2008;330:151-60.
[47] Fernandes M, Gama M, Dourado F, Souto AP. Development of novel bacterial cellulose composites for the textile and shoe industry. Microb. Biotechnol. 2019;12:650-61.
[48] Sekar N, Ramasamy RP. Electrochemical impedance spectroscopy for microbial fuel cell characterization. J Microb Biochem Technol S. 2013;6.
[49] Berthier F, Diard J-P, Michel R. Distinguishability of equivalent circuits containing CPEs: Part I. Theoretical part. J. Electroanal. Chem. 2001;510:1-11.
[50] Biffinger JC, Ray R, Little B, Ringeisen BR. Diversifying biological fuel cell designs by use of nanoporous filters. Environ. Sci. Technol. 2007;41:1444-9.
[51] Ko Y, Oh H, Lee H. Use of bacterial cellulose from Gluconacetobacter hansenii NOK21 as a proton-permeable membrane in microbial fuel cells. J Microb Biochem Technol. 2015;7:145-51.
[52] Wang Z, Lim B. Mixed cellulose ester filter as a separator for air-diffusion cathode microbial fuel cells. Environ. Technol. 2017;38:979-84.
[53] Marzorati S, Schievano A, Colombo A, Lucchini G, Cristiani P. Ligno-cellulosic materials as air-water separators in low-tech microbial fuel cells for nutrients recovery. J. Cleaner Prod. 2018;170:1167-76.
[54] Vilela C, Silva AC, Domingues EM, Gonçalves G, Martins MA, Figueiredo FM, et al. Conductive polysaccharides-based proton-exchange membranes for fuel cell applications: The case of bacterial cellulose and fucoidan. Carbohydr. Polym. 2020;230:115604.

Figure captions:

Fig. 1 (A) Fabrication procedure of MEA air-cathode based on BC, CNT and NZ and (**B)** SCMFC configuration in this work.

Fig. 2 (A) ATR-FTIR spectra of BC and BC-NZ, (**B)** EDX mapping and surface atomic distribution of BC-NZ, (**C)** XRD spectra and (**D)** Thermal stability behaviour of BC and BC-NZ.

Fig. 3 FESEM image and WCA of bare BC **(A)** and BC-NZ **(B)**, AFM image of bare BC **(C)** and BC-NZ **(D)**.

Fig. 4 (A) The role of BC-CNT-NZ in SMFC and the effect of WCA on MEA's performance, **(B)** DO and **(C)** Evaporation rate versus time.

Fig. 5 Nyquist plot of BC-CNT-NZ and GDE in frequency range of 100 KHz to 20 mHz.

Fig. 6 LSV **(A)**, CV **(B)** of BC-CNT-NZ and GDE at 10 mV/s in sludge, Power density and polarization of the SCMFC cells **(C)** and Polarization test of single electrodes **(D)**.

Fig. 7 (A) LSV at 5 mV/s and different rpm of CNT-GC RDE and corresponding Tafel and **(B)** K-L plot.

Fig. 8 Pulse power density of the SCMFC cells evaluated by GLV discharges with pulse time of: 2 s **(A)**, 1s **(B)**, 0.5 s **(C)** and 0.1 s **(D)**.

Captions of tables:

Table 1 Total crystalline index, lateral order index and hydrogen bond index of BC and BC-NZ

Table 2 Application of cellulosic materials in membrane and air-cathode of MFCs

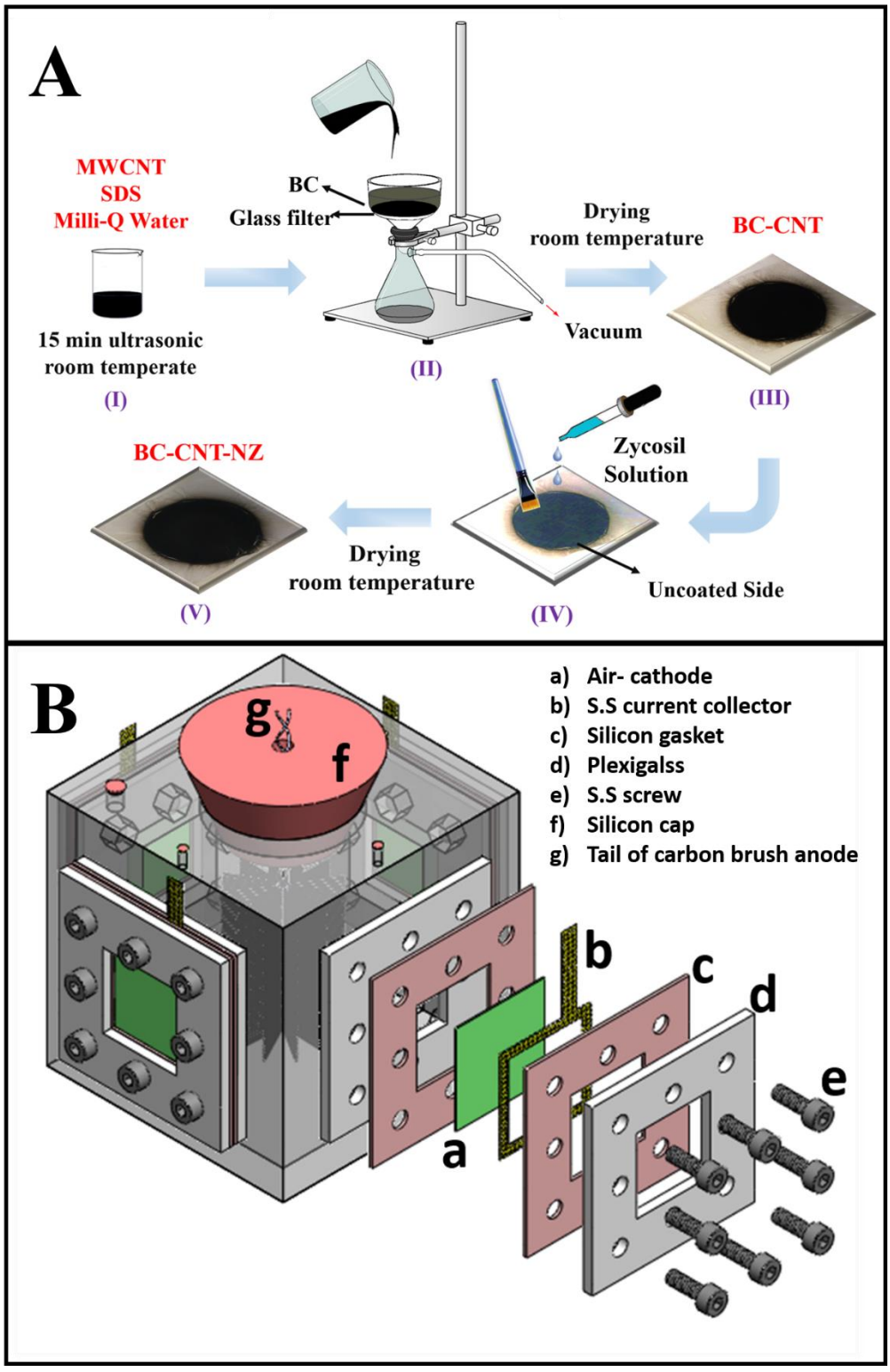
A
MWCNT
SDS
Milli-Q Water
15 min ultrasonic
room temperate
(I)
BC
Glass filter
(II)
Drying
room temperature
Vacuum
BC-CNT
(III)
Zycosil
Solution
Uncoated Side
(IV)
Drying
room temperature
BC-CNT-NZ
(V)
B
a) Air- cathode
b) S.S current collector
c) Silicon gasket
d) Plexigalss
e) S.S screw
f) Silicon cap
g) Tail of carbon brush anode
g
f
a
b
c
d
e

Fig.1

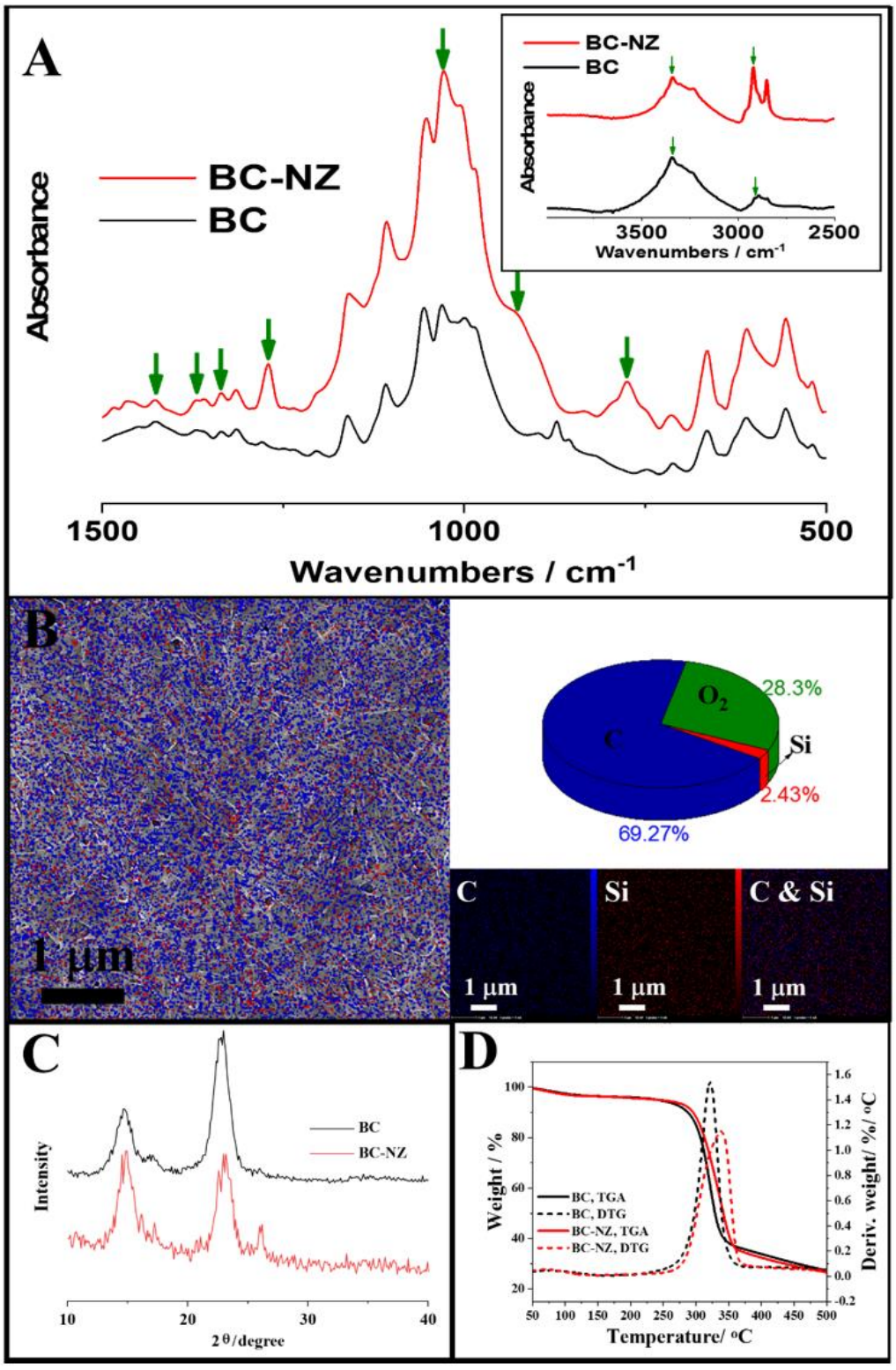
A
BC-NZ
BC
Absorbance
1500
1000
500
Wavenumbers / cm-1
3500
3000
2500
Wavenumbers / cm-1
B
1 μm
O2
28.3%
C
Si
2.43%
69.27%
C
Si
C & Si
1 μm
1 μm
1 μm
C
Intensity
BC
BC-NZ
10
20
30
40
2θ/degree
D
Weight / %
Deriv. weight/ %/ °C
BC, TGA
BC, DTG
BC-NZ, TGA
BC-NZ, DTG
Temperature/ °C

Fig. 2

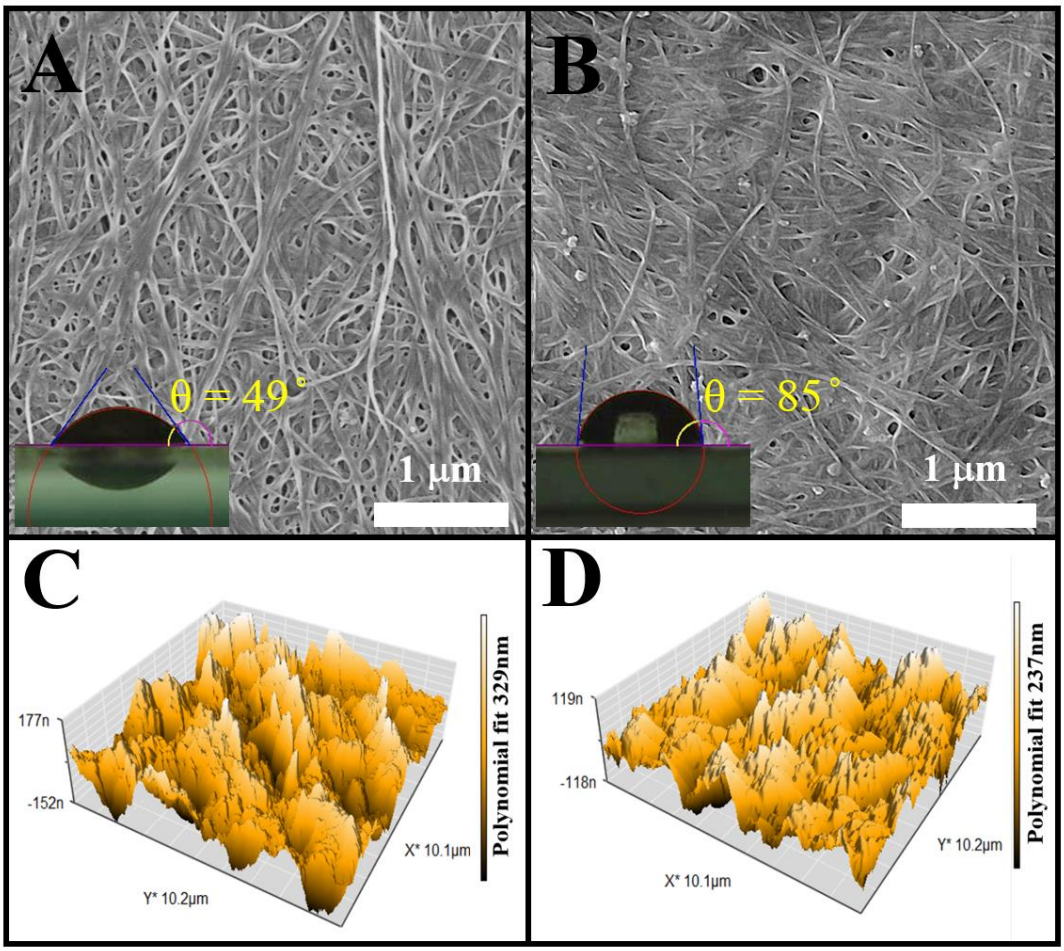
A
θ = 49°
1 μm
B
θ = 85°
1 μm
C
177n
-152n
X* 10.1μm
Y* 10.2μm
Polynomial fit 329nm
D
119n
-118n
X* 10.1μm
Y* 10.2μm
Polynomial fit 237nm

Fig. 3

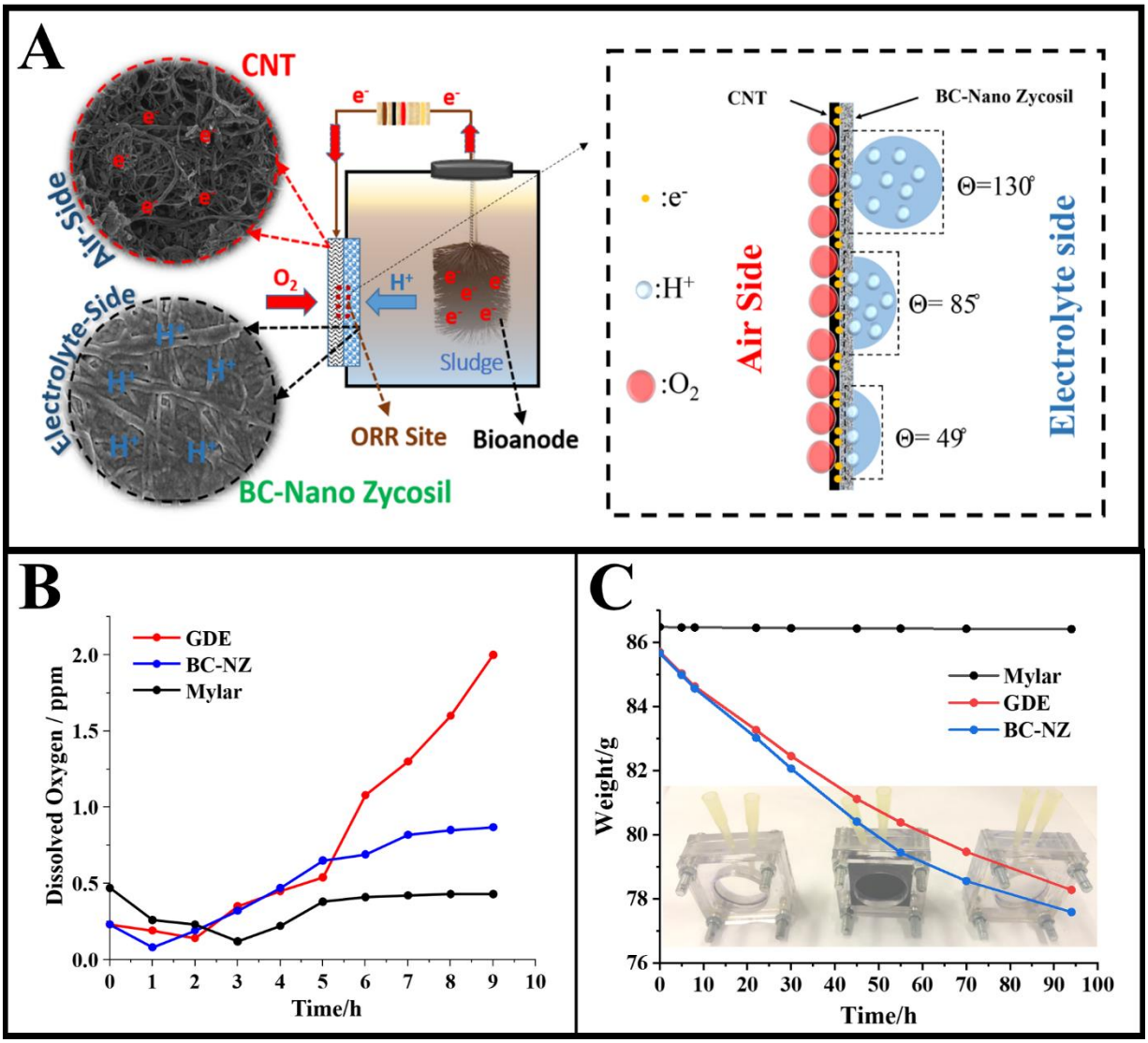
A
CNT
Air-Side
Electrolyte-Side
BC-Nano Zycosil
O2
H+
Sludge
ORR Site
Bioanode
:e-
:H+
:O2
Air Side
Electrolyte side
Θ=130°
Θ= 85°
Θ= 49°
B
GDE
BC-NZ
Mylar
Dissolved Oxygen / ppm
Time/h
C
Mylar
GDE
BC-NZ
Weight/g
Time/h

Fig. 4

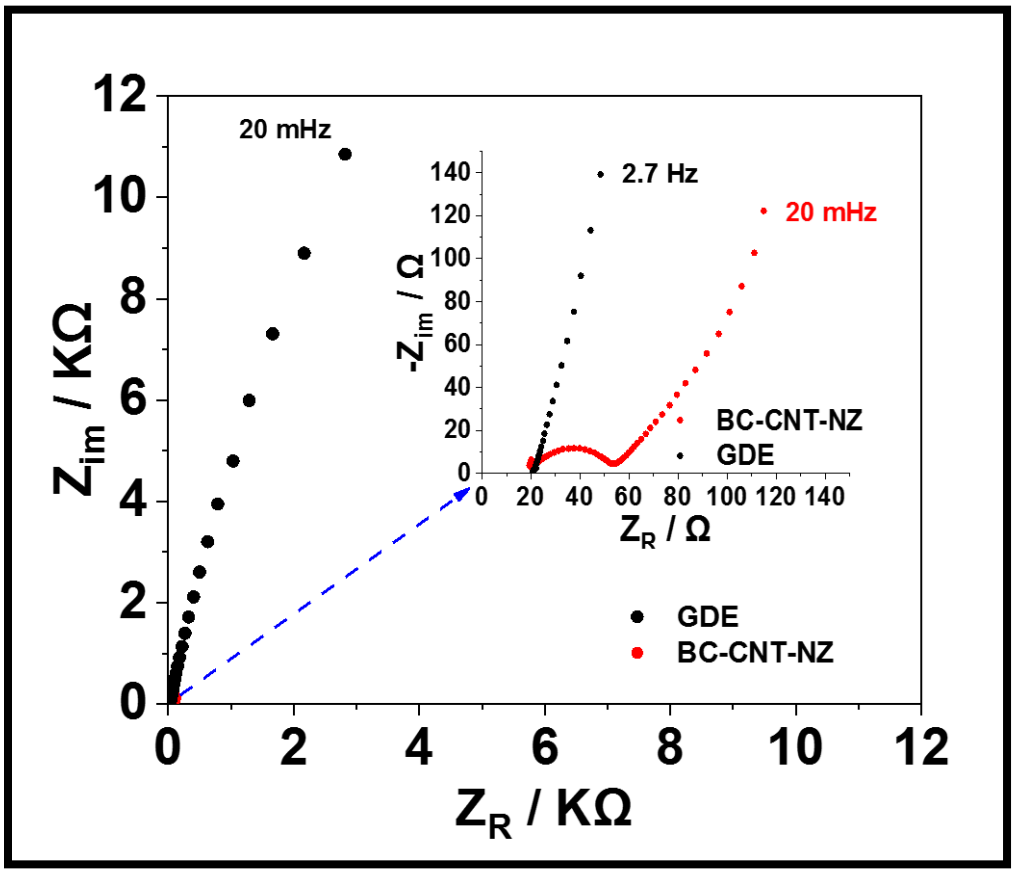
20 mHz
2.7 Hz
20 mHz
BC-CNT-NZ
GDE
GDE
BC-CNT-NZ
Z_{im} / KΩ
Z_R / KΩ
$-Z_{im}$ / Ω
Z_R / Ω

Fig. 5

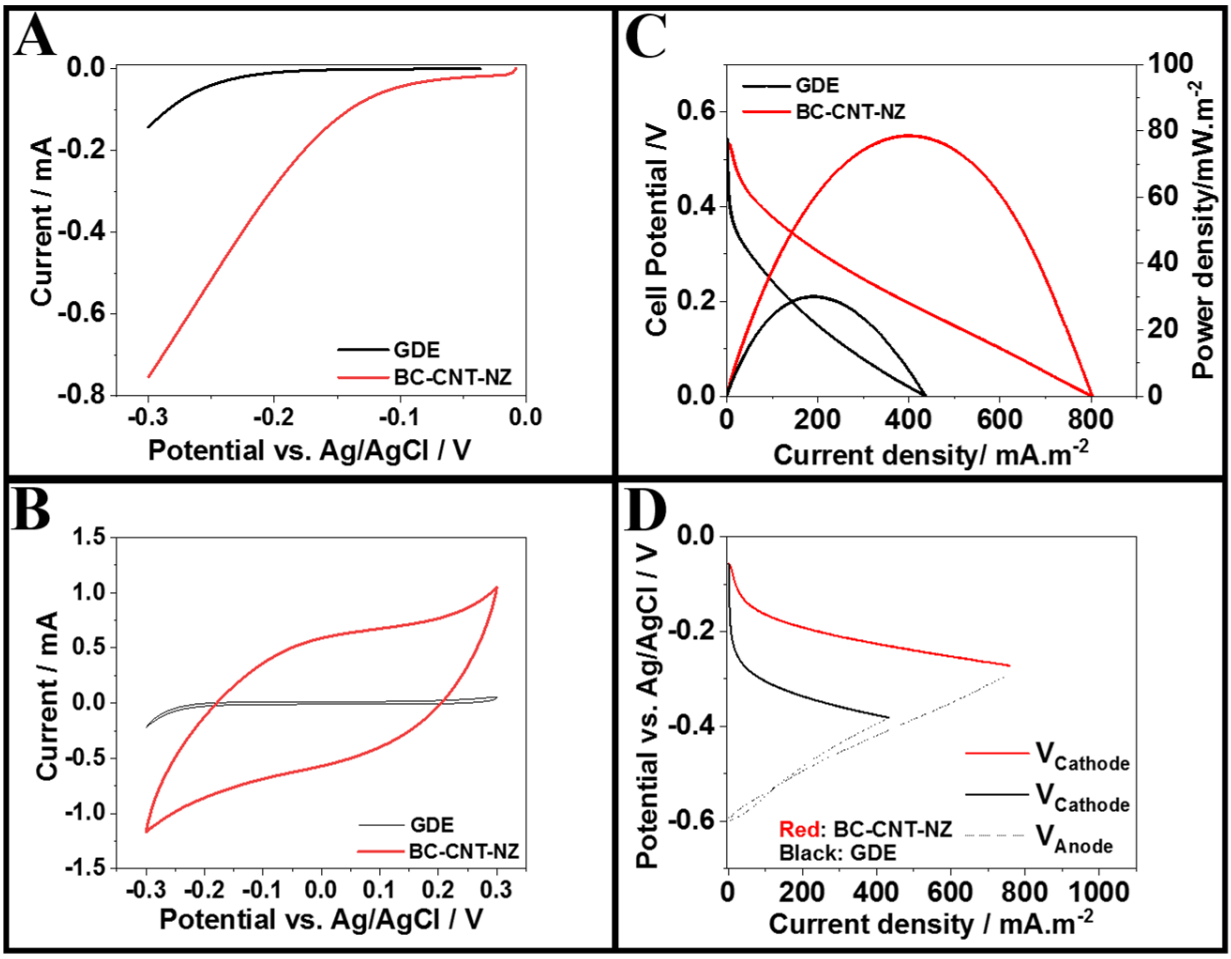
A
Current / mA
Potential vs. Ag/AgCl / V
GDE
BC-CNT-NZ
B
Current / mA
Potential vs. Ag/AgCl / V
GDE
BC-CNT-NZ
C
Cell Potential /V
Power density/mW.m-2
Current density/ mA.m-2
GDE
BC-CNT-NZ
D
Potential vs. Ag/AgCl / V
Current density / mA.m-2
VCathode
VCathode
VAnode
Red: BC-CNT-NZ
Black: GDE

Fig. 6

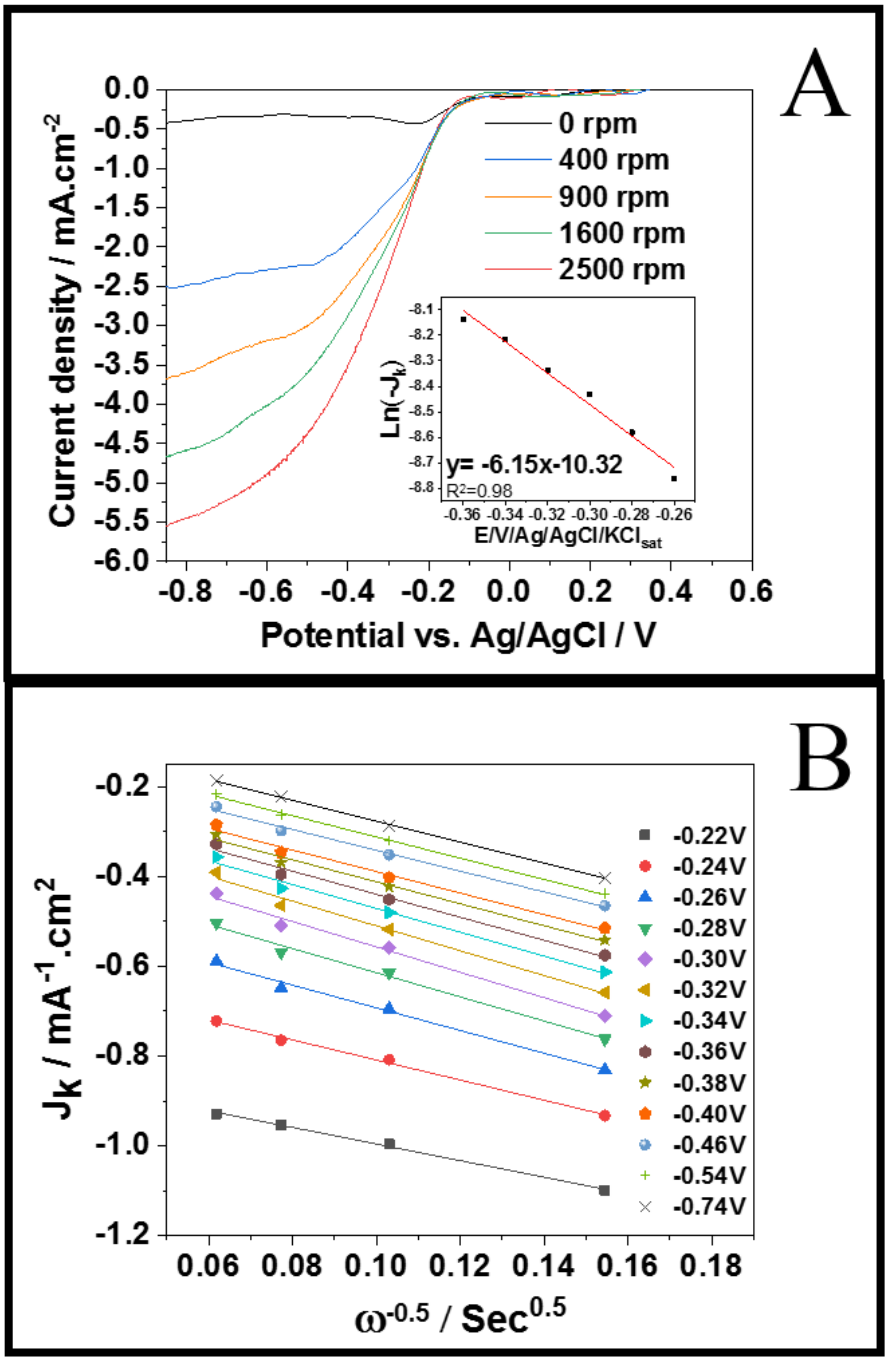
A
Current density / mA.cm-2
Potential vs. Ag/AgCl / V
0 rpm
400 rpm
900 rpm
1600 rpm
2500 rpm
Ln(-Jk)
y= -6.15x-10.32
R2=0.98
E/V/Ag/AgCl/KClsat
B
Jk / mA-1.cm2
ω-0.5 / Sec0.5
-0.22V
-0.24V
-0.26V
-0.28V
-0.30V
-0.32V
-0.34V
-0.36V
-0.38V
-0.40V
-0.46V
-0.54V
-0.74V

Fig. 7

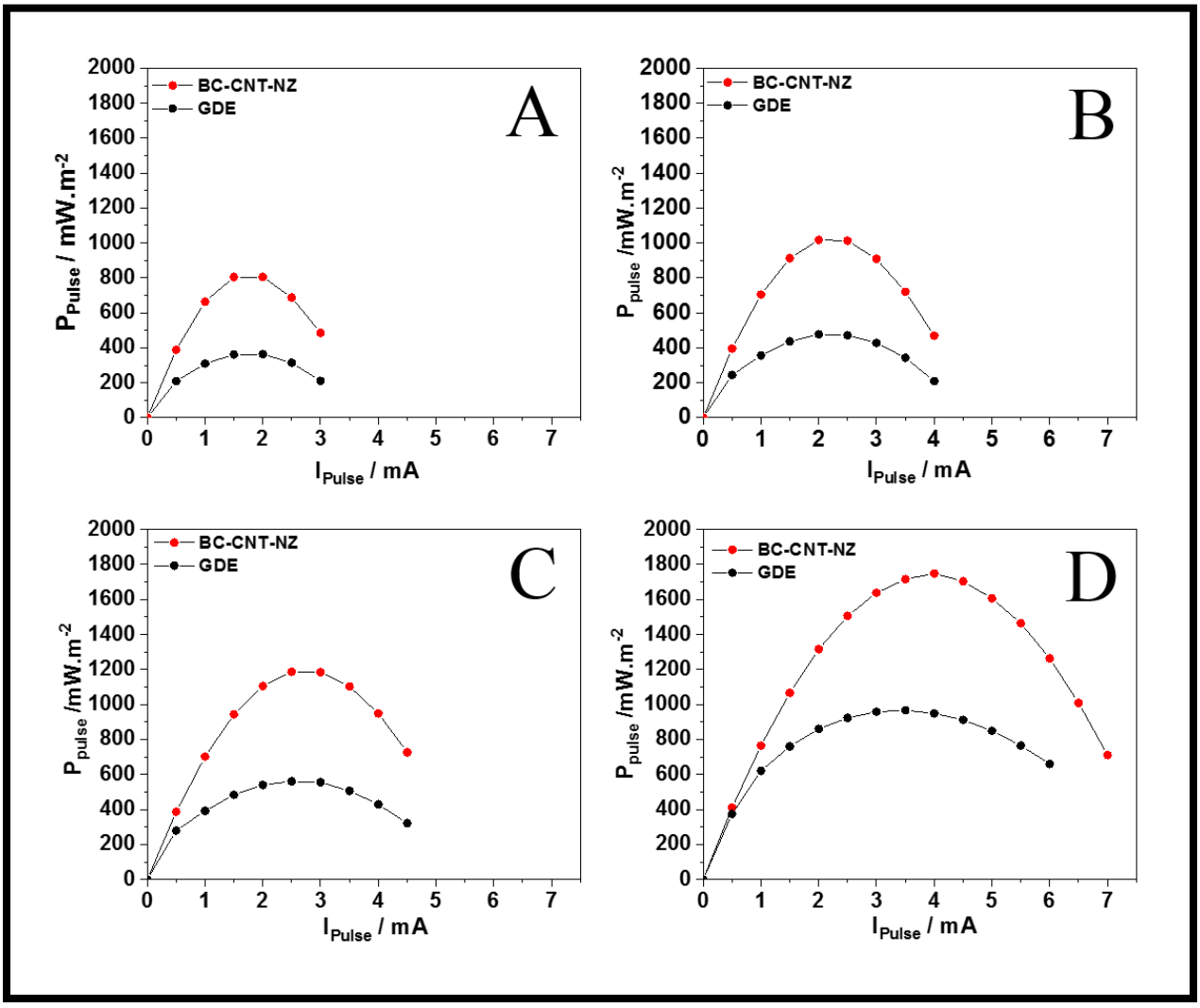
A
B
C
D
BC-CNT-NZ
GDE
P_{Pulse} / mW.m^{-2}
P_{pulse} /mW.m^{-2}
I_{Pulse} / mA
0
200
400
600
800
1000
1200
1400
1600
1800
2000
0
1
2
3
4
5
6
7

Fig. 8

Table 1

	TCI	LOI	HBI
BC	1.04	1.02	1.01
BC-NZ	0.97	0.85	1.01

Table 2

Cellulose membrane	Anode	Cathode	Configuration	Hydrophobic layer	Binder	Volume	Bacteria	Power density	Ref
Cellulose nitrate	graphite felt	Graphite felt	DCMFC	-	-	1.2 ml	*Shewanella oneidensis*	40 mW/m^2	[50]
BC	Carbon plate	Carbon plate	DCMFC	-	-	45 lit	Soil (mixed culture)	73-200 mW/m^2	[51]
-	Carbon felt	Carbon cloth-cellulosic GDL with platinum	SCMFC	Esterified cellulose nano fiber	Nafion	27 ml	Mixed culture	1518.3 mW/m^2	[11]
Mixed cellulose ester filter	Carbon brush	Commercial GDE with platinum 0.5 mg/cm^2	SCMFC	PTFE	-	250 ml	Anaerobic sludge	780.7 mW/m^2	[52]
Giant canes and Maize stalks cellulose	Carbon cloth	Carbon cloth GDE with carbon black	SCMFC	PTFE	PTFE	-	Swine manure of a pig-farm	44 mW/m^2	[53]
Poly(4-styrene sulfonic acid)/BC	Carbon brush	Carbon cloth GDE with platinum 0.1 mg/cm^2	SCMFC	PTFE	-	900 ml	*Shewanella frigidimarina*	2.42 mW/m^2	[54]
BC based MEA	Carbon brush	BC-CNT	SCMFC	NZ	Binder-less	250 ml	Mixed culture	80-1790 mW/m^2	This work

Declaration of interests

☒ The authors declare that they have no known competing financial interests or personal relationships that could have appeared to influence the work reported in this paper.

☐The authors declare the following financial interests/personal relationships which may be considered as potential competing interests:

Suggested Referees

Name	Affiliation	Email
Rafael Luque	University of Cordoba	rafael.luque@uco.es
Mehdi Tajvidi	School of Forest Resources, University of MAINE	mehdi.tajvidi@maine.edu
Alberto Figoli	Italian National Research Council	alberto.figoli@cnr.it ; a.figoli@itm.cnr.it
Stefania Specchia	Politecnico di Torino	stefania.specchia@polito.it
Barbara Mecheri	University of Rome Tor Vergata	barbara.mecheri@uniroma2.it
Clara Santato	Polytechnique Montréal	clara.santato@polymtl.ca
Plamen Atanassov	University of California, Irvine	plamen.atanassov@uci.edu
Mostafa Ghasemi	Universiti Teknologi PETRONAS	mostafghasemi@gmail.com
Deepak Pant	Flemish Institute for Technological Research, VITO, Belgium	deepak.pant@vito.be